

Enantiocontrolled macrocyclization by encapsulation of substrates in chiral capsules

Received: 4 February 2023

Accepted: 5 June 2023

Published online: 03 July 2023

 Check for updates

Linfeng Tan¹, Mo Sun¹✉, Huaxin Wang¹, Jiasheng Wang¹, Jehan Kim²
& Myongsoo Lee¹✉

Chiral macrocycles are commonly found in nature and have strong binding affinity to their targets. Thus, the development of efficient macrocyclization strategies is an important goal in the synthetic community. However, macrocyclization with chirality induction remains a great challenge because of the large entropic penalty associated with ring closure while maintaining the chiral conformation. Here, we report a highly efficient chiral macrocyclization with controlling enantioselectivity using a chiral confinement strategy. A linear substrate is encapsulated by a host precursor molecule through the formation of chiral capsule structures, which subsequently self-assemble into a robust two-dimensional structure entrapping the substrate with a folded chiral conformation. Then, the reaction under confinement generates an enantiopure macrocycle product. Furthermore, the chirality of the capsule assembly can switch into an opposite form using sonication, capable of controlling enantioselectivity. The substrate-encapsulating process is amenable to a substrate change, thus enabling diverse chirality induction in macrocycle formation. This macrocyclization method works with substrates decorated with a wide range of functional groups at high levels of precision and efficiency.

Chiral macrocycle molecules are abundant in nature and engender intriguing properties associated with immense conformational restrictions^{1–4}. Inspired by the challenging structures and potent biological activities of naturally occurring macrocycles, the development of efficient macrocyclization methods is an important target for, in particular, novel therapeutics. So far, some efficient methods for macrocyclizations have been developed^{5–8}; nevertheless, it is challenging to induce chirality because of the massive entropic penalties associated with ring closure together with maintaining chiral conformation⁹. Thus, efficient chirality induction in macrocyclization requires chiral constriction of a substrate by robust confinement to a chiral environment, and is rarely reported.

Although specific binding to an enzyme or a synthetic chiral catalyst have been applied to generate chirality during macrocycle formation^{10,11}, they are too specific to induce the desired chirality and these synthetic methods show a lack of switching capability. Thus,

universal chirality induction with enantiocontrol in macrocyclization remains largely unexplored. The main reason for this is that the ring-closing process requires dynamic control of chiral space simultaneously with robust chiral confinement^{12,13}. In most cases, however, directional interactions, such as hydrogen bonds and coordination bonds are employed for binding substrates to chiral auxiliaries, which are far from dynamic structural changes without bond breaking¹⁴. Except for a few cases¹⁵, confining chiral conformation inside chiral void spaces suffers from similar challenges because the interior walls consist of rigid frameworks that are not compatible with dynamic characteristics^{16–21}. Confinement of a substrate through elastic capsule formation of flexible chiral precursors through non-specific interactions would overcome this limitation, because the wrapping process by the chiral precursors would endow the capsule around the substrate with chiral bias that can be switched using external stimuli, as typically observed in dynamic self-assembly^{22,23}. Subsequently, the

¹Department of Chemistry, Shanghai Key Laboratory of Molecular Catalysis and Innovative Materials, Fudan University, Shanghai, China.

²Pohang Accelerator Laboratory, POSTECH, Pohang, Korea. ✉e-mail: mosun@fudan.edu.cn; mslee@fudan.edu.cn

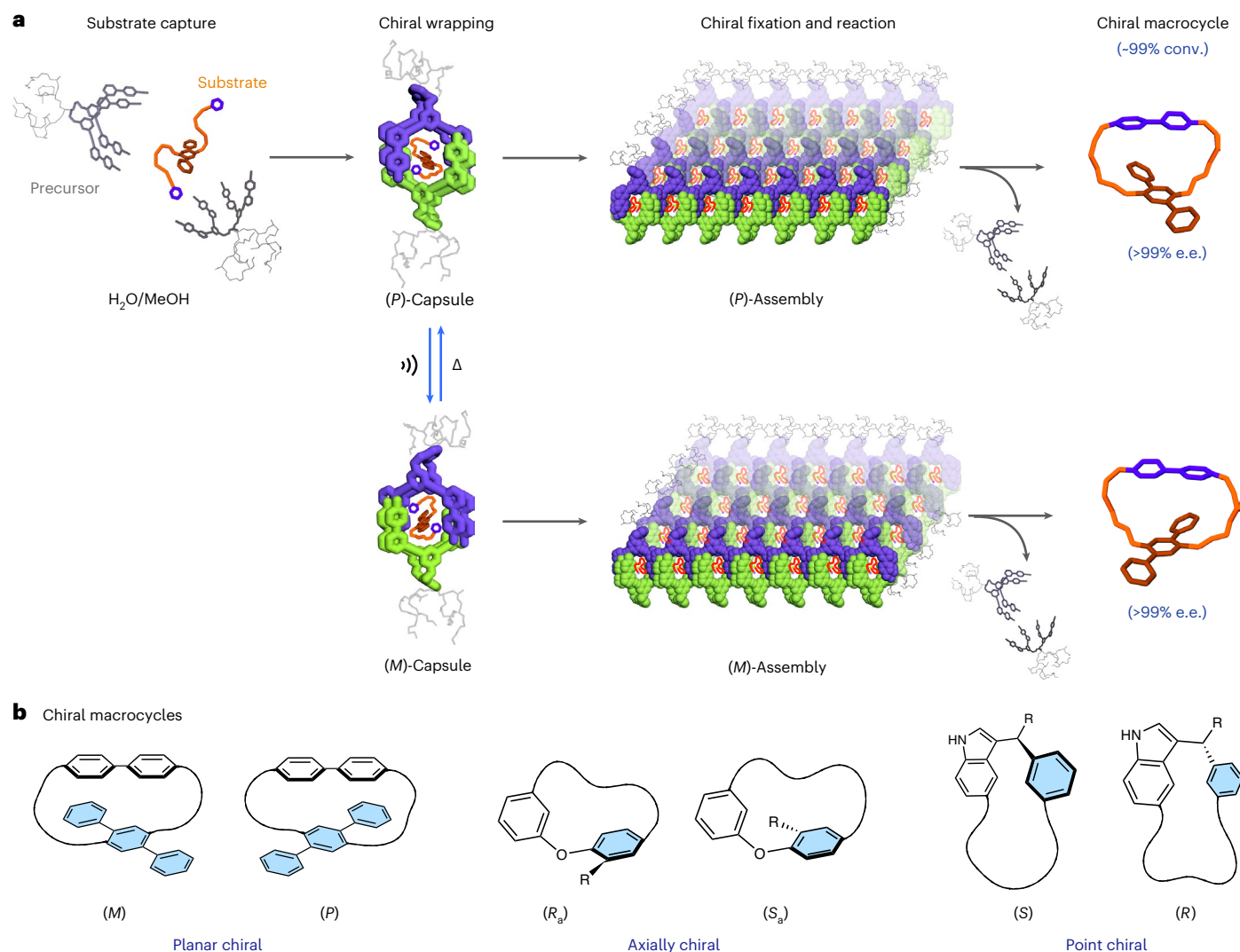


Fig. 1 | General concept of capsule formation for chiral macrocyclization.

a, Schematic representation of the formation of capsule assembly for chiral macrocycle synthesis. When a molecularly dissolved precursor molecule and a hydrophobic linear substrate are mixed together in aqueous methanol solution, the precursor molecule forms a chiral capsule structure entrapping the substrate inside through hydrophobic interactions. The chirality of the capsule is able to switch between (*P*) and (*M*) forms in response to external stimuli. Subsequently,

each chiral capsule self-assembles into a robust 2D sheet structure. As a result, the chemical reaction under confinement in each of the capsules generates a chiral macrocycle with controlled enantioselectivity. **b**, Diverse chiral macrocycles with enantioselectivity control that can be produced by the capsule assembly, from planar chiral, axially chiral to point chiral macrocycles. *R_a* or *S_a* labels the enantiomers with axial chirality, and *P* or *M* labels the enantiomers with helical chirality. Conv., conversion yield.

first-formed flexible chiral capsules can be frozen by the stepwise self-assembly in which the chiral conformation of the entrapped substrate would be fixed to transform into a chiral macrocycle. Thus, the substrate-induced chiral capsule would function as a flexible molecular reactor with adaptability to diverse substrates and chirality switching capability, to perform highly efficient chiral macrocyclizations of diverse substrates under confinement at ambient conditions and precise control of enantioselectivity using readily available physical forces. Here, we report substrate-induced flexible capsule formation, enabling a diverse range of substrates to transform into chiral macrocycles with precise control of enantioselectivity. Addition of a linear substrate into a molecularly dissolved flexible precursor solution triggers chiral capsule formation by encapsulating the substrate. This capsule subsequently self-assembles into a robust two-dimensional (2D) nanostructure, enabling the entrapped substrate to hold a uniform chiral conformation in each chiral space of the ordered nanostructure. As a result, the individual capsule units in the 2D structure act as a template and the stepwise self-assembly

of the capsules enables a collective chiral macrocyclization process to occur without noticeable error.

The flexibility for the formation of the first capsule enables the chiral space to be adaptive to various substrates with different functional groups, and allows the capsule that is encapsulating a substrate to undergo collective chirality switching, affording diverse chirality with controlled enantioselectivity. Compared with other catalytic systems, which tolerate only a specific reaction with incomplete conversion and are unable to control enantioselectivity^{10,11}, our system can tolerate various substrates and hence induce different chirality in macrocyclization with quantitative conversion and near-perfect enantioselectivity. In particular, the enantioselectivity can be precisely controlled by sonication (Fig. 1).

Results and discussion

Substrate-encapsulating capsule formation

The precursor molecule, **1**, which traps substrates, consists of a conformationally flexible, pyridine-based aromatic segment with a hydrophilic

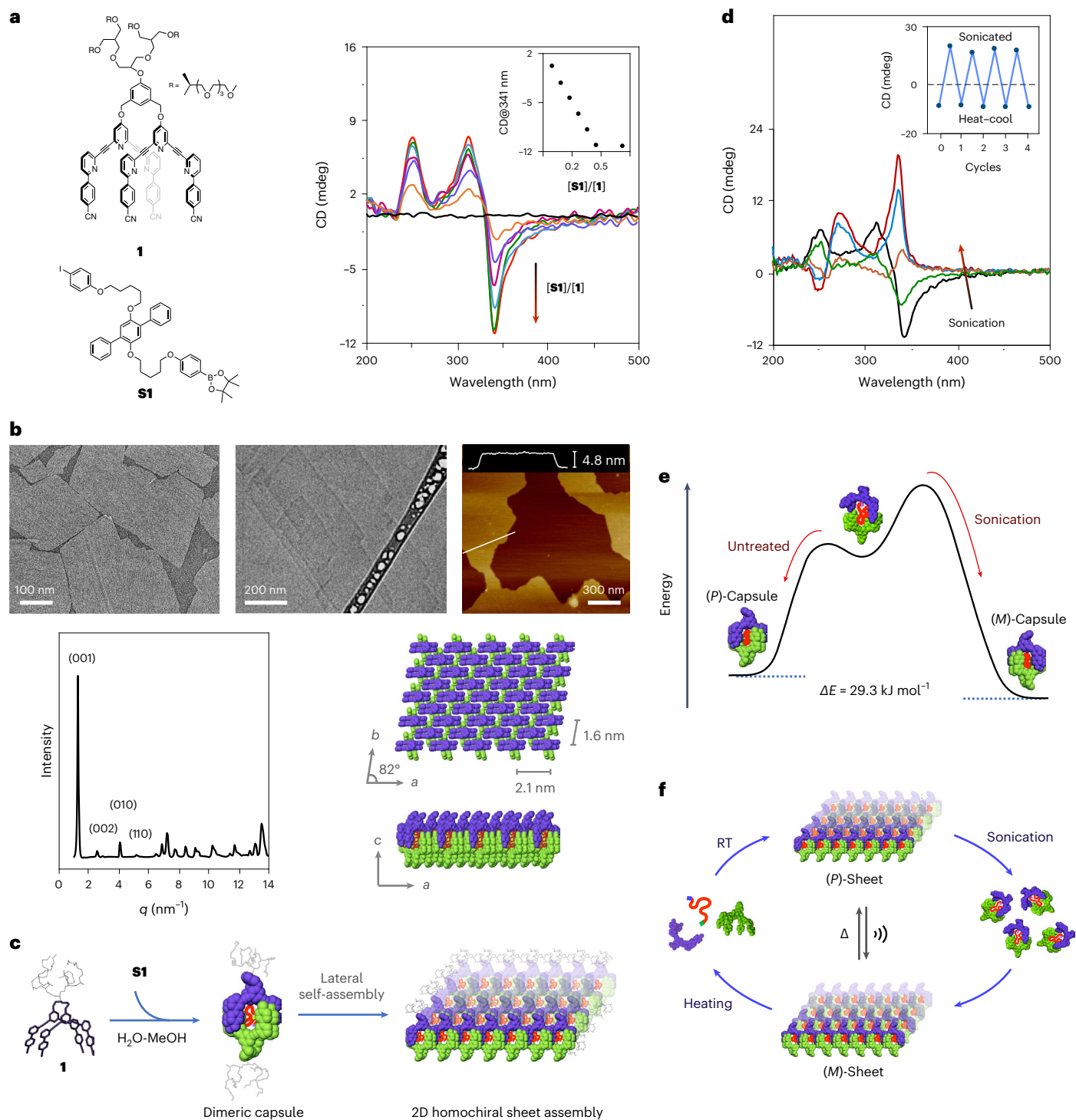


Fig. 2 | Formation of chiral capsule assembly and its chirality switching.

a, Chemical structure of precursor **1** and **S1**, and CD spectra of **1** with increasing **S1** at 50 μM . The inset is the plot of CD at 341 nm as a function of the equivalent of **S1**, indicating the formation of the **S1C1₂** complex with a 1:2 mole ratio.

b, Structural characterizations of the capsule assembly of **S1C1₂** including negative-stain TEM image, cryo-TEM image, AFM image and X-ray diffraction pattern (base-centred monoclinic structure with $a = 2.1$ nm, $b = 1.6$ nm, $c = 4.8$ nm and $\gamma = 82^\circ$).

c, Schematic representation of the self-assembly of substrate-induced dimeric capsules into a single-layered sheet structure. **d**, CD spectra of **S1C1₂** sheet solution on sonication and then ageing, showing CD inversion, from initial state (black curve), 10 min sonication (green curve), 30 min sonication

(orange curve), then ageing 30 min after sonication (blue curve) and ageing 50 min after sonication (red curve). The inset shows the consecutive CD cycles, indicative of reversible switching between (*P*)-assembly and (*M*)-assembly over four cycles (CD intensity at $\lambda = 337$ nm for heat-cool treatment, and $\lambda = 335$ nm for sonication). **e**, Calculated potential energy landscape, indicating that the (*P*)-capsule locked in the kinetically trapped state of the sheet assembly can be switched to a thermodynamically stable capsule on sonication. **f**, Schematic representation of a cycle from substrate trapping to form a (*P*)-sheet assembly, which, on sonication, transforms into an (*M*)-sheet assembly passing through breaking into dimeric capsules. Subsequent heat treatment regenerates the (*P*)-sheet assembly via a molecularly dissolved state.

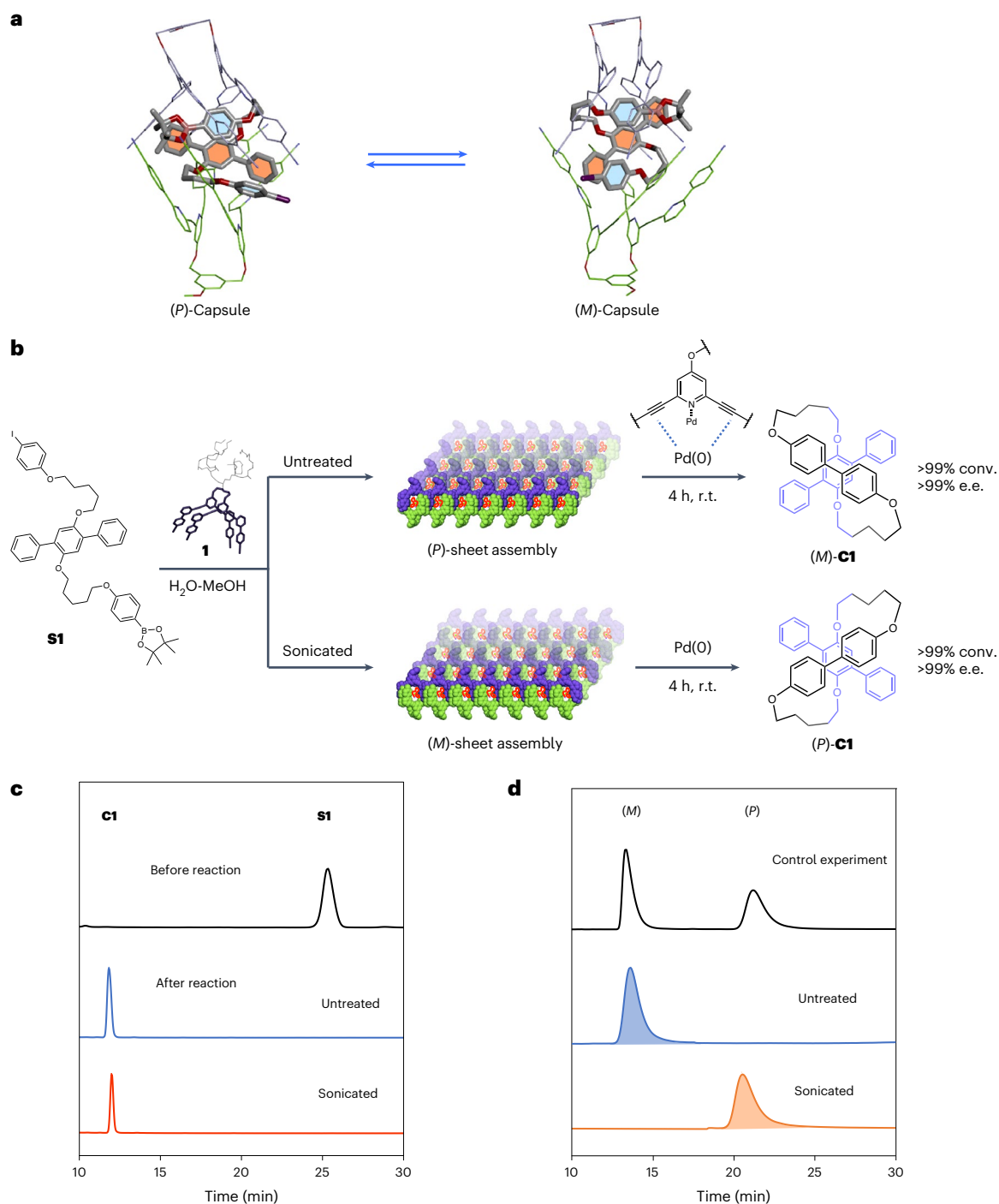
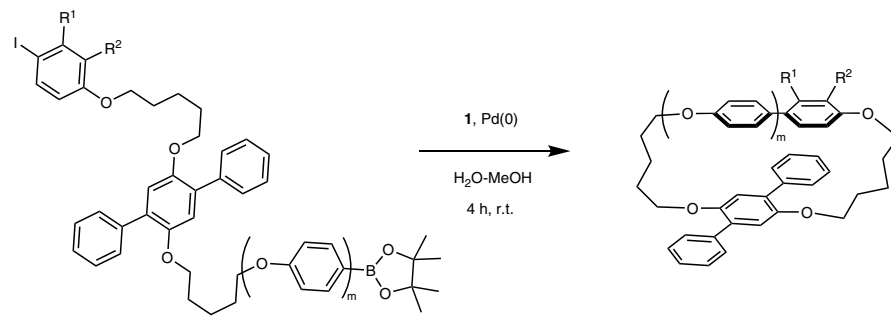


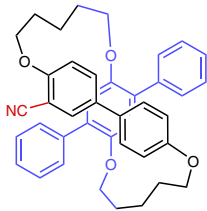
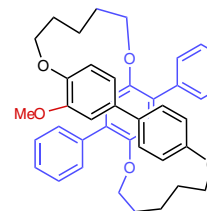
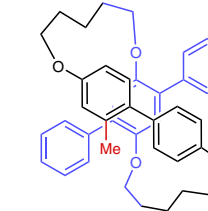
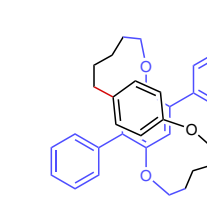
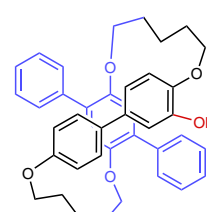
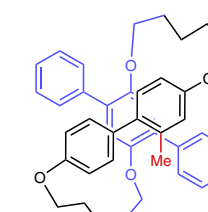
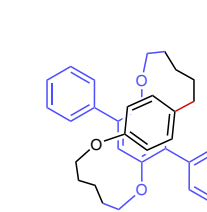
Fig. 3 | Chiral macrocyclization of **S1 in capsule assembly.** **a**, Simulated chiral conformations of **S1** in the chiral capsule of **S1C12**. **b**, Schematic representation of transformation of **S1** into **C1** in the capsule assembly of **S1C12** under different conditions. r.t., room temperature. **c**, HPLC traces obtained from the macrocyclizations of **S1** in the capsule assembly to yield **C1** before (top) and

after reactions in untreated (middle) and sonicated (bottom) solutions, showing quantitative conversions. **d**, Chiral HPLC traces of **C1** obtained from a solution reaction of **S1** in the absence of **1** (top), and in the **S1C12** sheet assembly of the untreated (middle) and sonicated (bottom) solutions.

chiral dendron (Fig. 2a). The pyridine units in the precursor can provide a potential binding site for diverse metal catalysts in confined reactions. Hydrophobic substrates can trigger **1** into a capsule-shaped molecular container through hydrophobic interactions together with additional dipolar interactions owing to cyanide (CN) groups at the end parts of the aromatic segments. The dimeric assembly with a chiral dendron positioned on its up and down apices can create a chiral interior by twisting in a preferred handedness due to chiral transfer from the hydrophilic chains. To investigate the substrate-induced chiral

self-assembly behaviour of **1**, we selected **S1** as a model hydrophobic substrate containing end groups for a Suzuki–Miyaura coupling reaction (Fig. 2a). Precursor **1** is not soluble in pure water and shows insufficient solubility for trapping hydrophobic substrates with the addition of up to 50% MeOH. Thus, we selected aqueous MeOH solution containing 60% MeOH as suitable for all of our investigations in this work. Indeed, with adding hydrophobic substrate **S1** into a solution of precursor molecule **1** (methanol/water = 6.0:4.0 v/v) at a concentration of 50 μM , the circular dichroism (CD) spectra showed the induction of

Table 1 | Scope of planar chiral macrocyclization in the capsule assembly of **1**


	S1a	S1b	S1c	S1d
R ¹	H	H	CH ₃	H
R ²	CN	OCH ₃	H	H
<i>m</i>	1	1	1	0
Untreated	 (M)-C1a 98% conv. >99% e.e.	 (M)-C1b 98% conv. >99% e.e.	 (M)-C1c >99% conv. >99% e.e.	 (M)-C1d 95% conv. >99% e.e.
Sonicated	 (P)-C1a 98% conv. >99% e.e.	 (P)-C1b 98% conv. >99% e.e.	 (P)-C1c >99% conv. >99% e.e.	 (P)-C1d 96% conv. >99% e.e.

a negative Cotton effect at higher wavelengths in the spectral range of the aromatic segment of the precursor. The CD signals increase with the content of the substrate up to a mole ratio of 1:2, (**S1c₂**). Thus, the hydrophobic substrate can induce the formation of a dimeric chiral capsule around a substrate with a preferred handedness (Fig. 1b and Supplementary Table 1). The encapsulation of the substrate by **1** was further confirmed by ¹H NMR spectroscopic measurements, which showed upfield shift of the resonance peaks associated with the aromatic protons of both **1** and **S1** (Supplementary Fig. S9).

The dimeric capsule (**S1c₂**) with hydrophilic up and down, and hydrophobic side, faces can be laterally associated through side-by-side hydrophobic interactions to form a 2D structure. This was confirmed by transmission electron microscopy (TEM) measurements (Fig. 2b). The image obtained from a cast film shows nanosheets with a sizeable area with well-defined straight edges, ranging in their lateral dimensions from submicrometres to several micrometres, and indicating that the dimeric chiral capsule self-assembles into an ordered 2D structure,

which maintains its well-defined 2D shape in bulk solution, as confirmed by cryo-TEM. Atomic force microscopy (AFM) investigations revealed that the self-assembled sheets are very flat and uniform, with a thickness of 4.8 nm. The formation of a highly ordered structure was confirmed by X-ray diffraction, which showed a number of sharp reflections corresponding to a base-centred monoclinic superlattice, indicating that the single-layered sheets consist of an ordered 2D arrangement of the dimeric capsules with dimensions of *a* = 2.1 nm and *b* = 1.6 nm (Fig. 2b and Supplementary Table 2). The results demonstrate that a substrate induces the formation of a chiral dimeric capsule that laterally associates to form a highly ordered, single-layered sheet structure entrapping the substrate inside (Fig. 2c). With the absence of the substrate, precursor **1** forms only small irregular aggregates with a lack of any noticeable Cotton effect, which is further supported by X-ray measurements showing only a broad halo (Supplementary Fig. S60).

Taken together, these observations indicate that the molecularly dissolved **1** can self-assemble into a dimeric capsule assembly only by

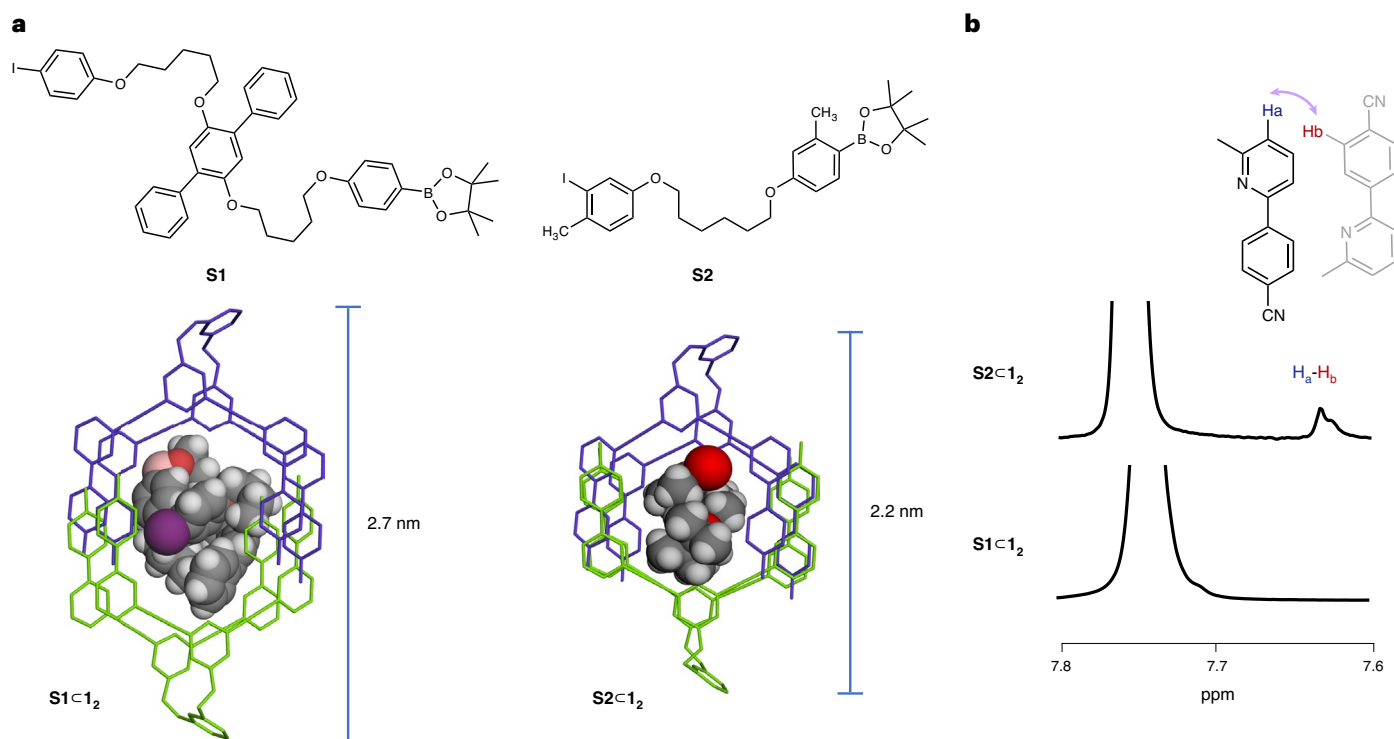


Fig. 4 | Adaptability of capsule to substrate changes in size. **a**, Schematic representation of the dimeric capsules of **1** entrapping **S1** (left) and **S2** (right). The dimeric capsule is adaptable to the size change of the substrate by means of flexibly squeezing its internal space. Considering the reduction in the layer thickness obtained from AFM measurements, the heights of the dimeric capsule

are estimated by the CPK model using Discovery Studio software. **b**, Partial one-dimensional NOE NMR signals of **S1C1₂** and **S2C1₂**, showing that NOE correlation is induced at 7.6 ppm in **S2C1₂**, in contrast to **S1C1₂**. This result indicates that the dimeric capsule of **1** is shrunk when entrapping a smaller substrate.

entrapping a hydrophobic substrate. Therefore, it can be considered that the encapsulation efficiency of the capsule units in the sheet assembly is nearly perfect. Additionally, this implies that the size of substrates for the capsule formation should be compatible with the hollow cavity of the capsule, because larger substrates than the inside of the capsule would disturb the formation of the dimeric capsule.

Notably, when the solution of **S1C1₂**-sheet assembly was subjected to ultrasonication for 60 min in an ice-water bath, the CD signal at longer wavelengths was inverted from the negative minimum to a strong positive Cotton effect (Fig. 2d), while maintaining well-defined 2D sheet structures (Supplementary Fig. 61), thus demonstrating that the capsule assembly has highly dynamic chirality in response to a physical force. Upon heating to 43 °C and then cooling to room temperature, the CD signal returns back to the negative Cotton effect, indicative of pathway-dependent chirality inversion. To gain insight into the switching mechanism, we performed force-field calculations using Schrödinger software, which gave rise to relaxed structures (Supplementary Figs. 62 and 63). The calculations showed that the (*M*)-capsule is a thermodynamically favoured structure with an equilibrium constant (K_{eq}) of 1.2×10^5 (Fig. 2e). Indeed, when the untreated solution was diluted up to 5 μ M to maintain a stable dimeric capsule structure without further assembly into 2D sheets and then ageing for 30 minutes, a sufficiently long time to form a more stable dimeric capsule, the solution showed a positive CD signal (Supplementary Fig. 64a), supporting that the (*M*)-structure with a positive Cotton effect exists in a thermodynamically stable state. On the other hand, the concentrated solution (50 μ M), the condition for rapidly forming a 2D sheet structure, exhibits a negative CD signal, suggesting that the kinetically controlled (*P*)-dimeric capsule is frozen into 2D sheet assembly before reaching a thermodynamic equilibrium²⁴. Upon sonication, the kinetically trapped 2D structure disassembles into individual capsule

units that establish a dynamic equilibrium with a thermodynamically stable capsule. As a result, the stable capsule re-assembles into a 2D sheet structure with opposite chirality (Fig. 2f). The evidence for maintaining the integrity of the dimeric capsule units when sonication is applied is provided by TEM and dynamic light scattering measurements (Supplementary Fig. 64b,c). Upon heating the sonicated solution, however, the stable (*M*)-sheet assembly is dissolved to its molecular components (Supplementary Figs. 64d,e and 65a), which regenerates (*P*)-sheet structures upon cooling to room temperature (Supplementary Fig. 65b). This result suggests that the (*P*)-capsule locked in the kinetically trapped state can be converted to a thermodynamically stable structure only after sonication. The subsequent sonication recovers a positive maximum in the CD intensity at a wavelength of 335 nm, indicative of reversible switching in chirality over multiple cycles (Fig. 2d, inset, and Supplementary Fig. 66).

The chiral capsules solidified by stepwise 2D self-assembly enable the entrapped linear substrate to adopt a fixed chiral conformation, which can be switched in a collective manner triggered by external stimuli²⁵, thereby changing enantioselectivity in a macrocyclization process. Indeed, simulations showed that linear substrate **S1** confined in the chiral space adopts a folded chiral conformation in which the reactive end groups are positioned on the same side of the triphenylene plane (Fig. 3a), as supported by 2D nuclear Overhauser effect (NOE) measurements (Supplementary Fig. 67). *P*-(**S1C1₂**) confines the substrate to hold one chiral conformation, while the (*M*)-capsule gives rise to a conformation with an opposite chiral plane, indicating that the dynamic switching of the capsule can force chirality inversion of the substrate simultaneously. The collective chirality switching with an entrapped substrate was additionally confirmed by control CD experiments of **1** encapsulating an achiral dye substrate (**S5**), which exhibited induced CD signals associated with the dye at a separated wavelength range from **1** (Supplementary Fig. 68).

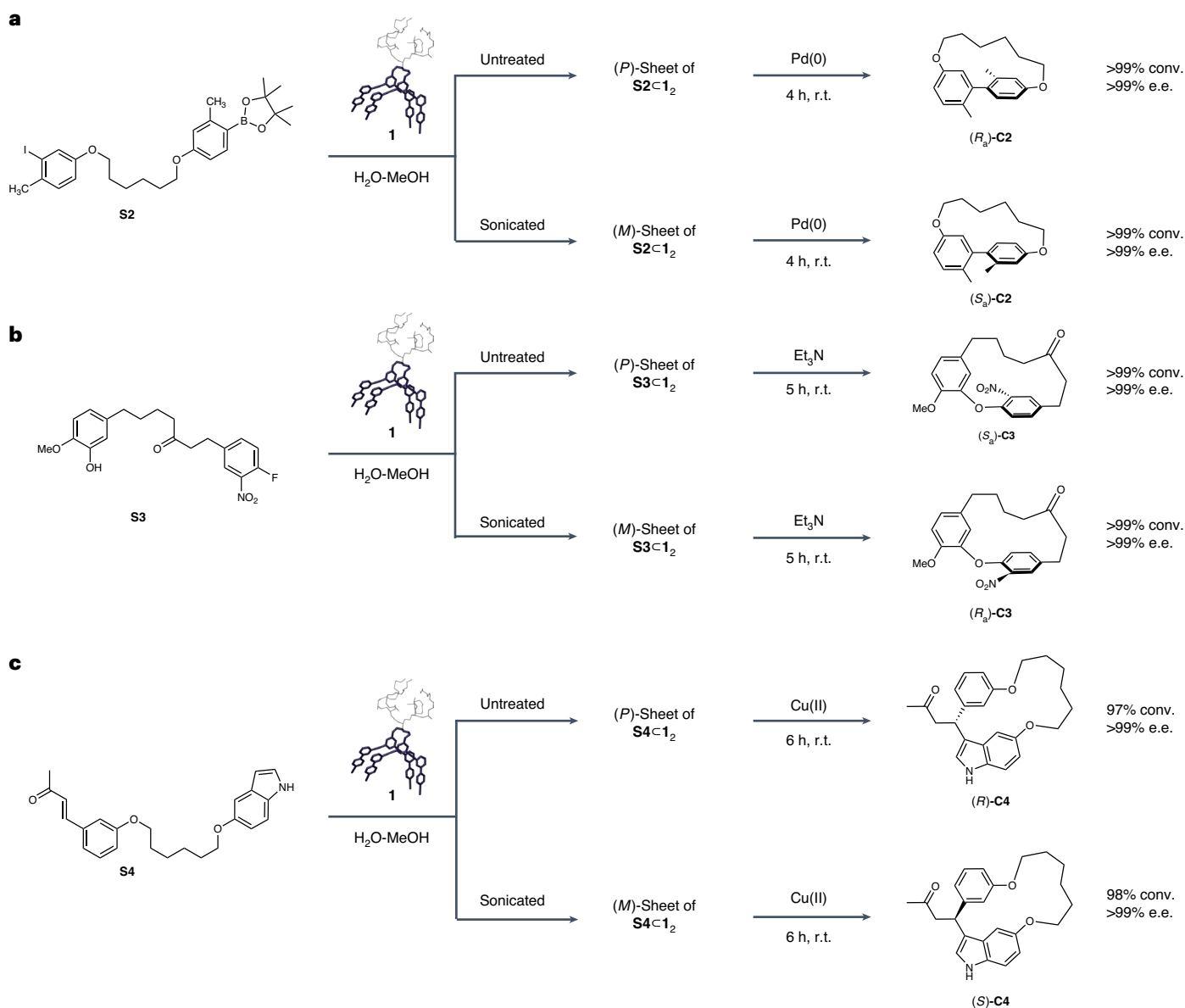


Fig. 5 | Diverse chiral macrocyclizations in capsule assembly.

a, Suzuki–Miyaura reactions of the smaller substrate **S2** in the capsule assembly (**S2C1₂**), showing the adaptivity of the elastic capsule assembly to a substrate change in size, while producing axially chiral macrocycles without compromising the performance in conversion and enantioselectivity. **b**, S_NAr reactions of **S3**

in the capsule assembly (**S3C1₂**), producing axially chiral macrocycles with quantitative conversions and controlled enantioselectivity. **c**, Michael reactions of **S4** in the capsule assembly (**S4C1₂**), giving rise to point chiral macrocycles with controlled enantioselectivity.

Chiral macrocyclization

This prompted us to consider that the covalent stitching of the end parts of **S1** in the capsule self-assembly would be an efficient synthetic method for generating a planar chiral macrocycle. To address this challenge, we added a catalytic amount of Pd(0), a single additional peak corresponding to a macrocycle product was identified in the analytical high-performance liquid chromatography (HPLC), for which the peak intensity increases gradually at the expense of **S1** and then levels off at 4 hours with traceless side peaks (Supplementary Fig. 69), indicating that the confined reaction produces a clean cyclized product with quantitative conversion (Fig. 3c). Notably, the macrocyclization proceeds with excellent enantioselectivity (>99% enantiomeric excess (e.e.)), as traced by chiral HPLC (Fig. 3d). The obtained profile shows only a single peak associated with the pure (*M*)-enantiomer of the macrocycle,

demonstrating that the cyclization gives rise to precise asymmetric induction. Considering the simulation results with substrate-induced self-assembly exhibiting the collective chirality inversion, the aromatic coupling reaction under identical conditions was performed with the solution after sonication. In sharp contrast, the reaction yields an enantiopure macrocycle, but with an inversion in enantioselectivity (Fig. 3d). This result demonstrates that the capsule assembly enables the entrapped substrate to efficiently transform into a planar chiral macrocycle in which the enantioselectivity can be precisely controlled using a physical force. It is noteworthy that the chiral sheet structures are preserved even after completing the chemical reaction (Supplementary Fig. 71), which is indicative of the robustness of the trapping assembly at ambient temperatures. Heating the solution, however, disintegrates the sheet structures (Fig. 2f), releasing the product and thereby establishing reaction cycles, as exemplified by dynamic self-assembly systems^{26–28}.

To investigate whether the confined macrocyclization in the capsule assembly could tolerate functionalized aryl halides, we prepared three different aryl iodide substrates that have an electron-withdrawing (**S1a**), electron-donating (**S1b**) and sterically hindered *ortho*-methyl group (**S1c**) (Table 1). A series of functionalized aromatic halides were well tolerated in the macrocyclization process without loss of conversion and enantiopurity. We also demonstrated that the coupling reaction of a substrate with an aliphatic boronate ester (**S1d**) afforded an enantiopure macrocycle product with controlled enantioselectivity by sonication.

Because of the elasticity of the non-specific interactions responsible for its capsule formation, the chiral space can flexibly change its size, thereby enabling the chiral space to tolerate different substrates to induce various chirality, which is different from inflexible chiral cages or containers based on hydrogen bonds or coordination bonds^{16–18}. To investigate the self-assembling behaviour of **1** induced by substrates with size changes, we selected **S2** with a large reduction in molecular size as an example (Fig. 4a). Similar to **S1**, CD measurements showed the induction of a negative Cotton effect at higher wavelengths at a mole ratio of 1:2 (Supplementary Fig. 77), demonstrating that a smaller substrate can also induce the formation of a dimeric chiral capsule that self-assembles into a well-defined 2D structure (**S2c1₂**-sheet assembly) with straight boundaries (Supplementary Fig. 77), but with apparent reduction in thickness from 4.8 nm to 4.2 nm, indicative of the shrinkage of the capsule while maintaining ordered 2D sheet assembly. The thickness reduction is attributed to sliding the aromatic segments of the dimeric capsule relative to each other to fit into the substrate with a decrease in size, as supported by NOE measurements (Fig. 4b and Supplementary Fig. 78).

To examine whether the aromatic coupling reaction of **S2** could induce different chirality from that of **S1**, we performed the confined reaction in **S2c1₂**-sheet assembly solutions to produce an axial chiral macrocycle (Fig. 5a). The reaction yields a highly enantiopure macrocycle product (Supplementary Fig. 79), indicating that the substrate-encapsulating approach is an excellent method for atroposelective macrocyclization. Similar to that of **S1c1₂**, the enantioselectivity can also be precisely controlled by sonication. On sonication, the reaction yields a macrocycle with opposite chirality (*S_a*-isomer) without any noticeable loss of enantiopurity (Supplementary Fig. 79). The remarkable performance in axial chirality induction and stereoselectivity switching is attributed to the adaptive binding to the chiral cavity in which robust stepwise homochiral self-assembly forces the substrate to fit into the uniform chiral environment. Indeed, dynamics simulations showed that the (*P*)-capsule stabilizes one atropisomeric conformer to generate the *R_a*-macrocycle (*R_a*-**C2**), while the (*M*)-capsule affords the other conformer (Supplementary Fig. 80), which explains the control of enantioselectivity in axially chiral macrocyclization by switching the chirality of the capsule assembly. This result demonstrates that the first-formed capsule is highly flexible to readily adapt to substrates with different sizes by capsule sliding, enabling the substrate to hold a fixed chiral conformation in the capsule, and thereby converting the substrates into atroposelective macrocycles with excellent efficiency and precision.

To confirm the generality of atroposelective macrocyclization in the chiral capsule, we investigated an *S_NAr* reaction using a linear substrate **S3** in the capsule (Fig. 5b). It should be noted that an enantioselective cyclization is a key step for the asymmetric synthesis of natural products, however, achieving high enantioselectivity in macrocyclization still remains a great challenge²⁹. This can be solved by the substrate-encapsulating approach. Indeed, amine-catalysed reaction in **S3c1₂**-sheet assembly produces an enantiopure macrocycle product in quantitative conversion (Supplementary Fig. 82). Consistent with CD inversion (Supplementary Fig. 81), the solution treated with sonication gives rise to a chiral macrocycle with opposite chirality without sacrificing the performance in conversion and enantioselectivity.

This result indicates that the substrate-encapsulating strategy can produce planar chiral macrocycles with diverse chiral planes from different chemical reactions.

In addition to axial chirality, we also investigated whether the capsule assembly induces a switchable stereocentre in macrocyclization, using a linear substrate (**S4**) containing an α,β -unsaturated carbonyl group at one end and an indole group at the other end for Michael addition (Fig. 5c)¹⁹. The reaction in **S4c1₂**-sheet assembly yields an enantiopure macrocycle with *R*-configuration at the stereocentre. In contrast, the macrocyclization after sonication produces the *S*-macrocycle product with opposite chirality (Supplementary Fig. 84), demonstrating that the capsule can also accurately induce point chirality with controlled enantioselectivity. From these observations, it is remarkable that our substrate-trapping strategy provides not only highly precise performance in chirality induction and chirality switching, but also a considerable general chiral macrocyclization method that is compatible with a broad range of linear substrates grafted with diverse functional groups to induce different chirality.

Conclusions

The high level of efficiency and precision of our capsule assembly for chirality induction in diverse macrocyclizations could be attributed to the robust fixation of elastic capsules into ordered 2D homochiral self-assembly, as reflected by TEM and X-ray observations (Fig. 2b). We have previously demonstrated that the ordered 2D self-assembly of non-covalent chiral pores can give rise to porous structures with near-perfect enantiopurity³⁰. On one hand, the tight confinement of substrates into the chiral capsule assembly would force the substrate to hold a uniform chiral conformation in each chiral space, capable of precise induction of topo-controlled chirality in collective macrocyclization without noticeable error^{31,32}. On the other hand, the flexibility of non-specific interactions responsible for the first capsule formation enables the individual capsules, not only to be highly adaptive to various substrates, but also to undergo chirality switching, affording desired chirality with or without stereocentres in macrocyclization. This unique performance with enantiocontrol differentiates the substrate-encapsulating system from natural enzymes and inflexible containers, including chiral auxiliaries, which are too specific for widespread use and, in most cases, lack a switching capability^{9–11,16–18}. We anticipate that our strategy, first substrate trapping and then robust fixation with high order, will provide access to a universal synthesis method guiding complex macrocycles containing multiple chirality with exquisite stereocontrol using readily available physical forces, which is necessary for a wide variety of applications, including drug discovery and nanotechnology.

Methods

Sample preparation

Related substrates (**S1–S5**) and **1** of 1:2 ratio were first mixed in methanol. Then, a certain amount of water was added gradually into the mixture to form a 60% methanol:water solution containing 25 μM related substrates and 50 μM **1**. The solution was subsequently treated without sonication at room temperature (untreated solution) or with sonication in an ice–water bath for 1 h (sonicated solution). The sample solution **Snc1₂** was finally stabilized for another 1 h before conducting the experiments.

Transmission electron microscopy

A drop of the sample solution was placed on a carbon-coated copper grid. After 1 min, the solvent was removed using filter paper. Then, the grid was stained by depositing a drop of uranyl acetate aqueous solution (1.0 wt%). The dried specimen was observed using a JEOL 2100 Plus instrument operated at 200 kV. The cryo-TEM experiments were performed with a JEOL 2100 Plus instrument operated at 200 kV using a Gatan 626 cryoholder.

Atomic force microscopy

The sample solution was dropped on the fresh mica surface directly and then the measurements were conducted on MultiMode 8 AFM in the air at ambient temperature using the peak force tapping mode.

Dynamics simulations

The calculated energy levels were obtained using Schrödinger Suites (Schrödinger) with MacroModel and Desmond modules. The total energy values of the complexes of **1** with **C1**, **S1** and **S2** were simulated as follows: first, through system builder and energy minimization using Desmond modules (parameters: force field: OPLS4; simulation time: 100 ps), we obtained the initial conformations of host–guest complexes with relatively low energies for the next-step molecular dynamics simulation; then, through molecular dynamics and minimization of MacroModel module (parameters: force field: OPLS4; solvent: e 50.9; cutoff: none; minimization method: PRCG; maximum iterations: 2,500; convergence on: gradient; convergence threshold: 0.05; dynamics method: stochastic dynamics; simulation temperature: 300.0 K; time step: 1.5 fs; equilibrium time: 1.0 ps; simulation time: 10,000 ps;) with constrained positions of **1**, we obtained the total energy values and configurations of the host–guest assemblies of *P/M-1* with different conformations of **C1**, **S1** and **S2**.

Circular dichroism

The experimental CD spectra were obtained using a JASCO J-810 spectrophotometer. The simulated CD spectra were simulated using Schrödinger Suites (Schrödinger). We input the enantiomeric chemical structures of **C1–C4** to calculate their CD spectra using VCD Spectra of the Jaguar module (parameters: electronic circular dichroism; use conformational search; force field: OPL4; solvent: none). Using the comparison of the experimental and simulated CD spectra of the cyclic products (**C1–C4**), the absolute conformations of the related compounds were assigned in the synthetic sections.

Data availability

The data that support the findings of this study are available in the Supplementary Information.

References

1. Heinis, C. Tools and rules for macrocycles. *Nat. Chem. Biol.* **10**, 696–698 (2014).
2. Campos, K. R. et al. The importance of synthetic chemistry in the pharmaceutical industry. *Science* **363**, eaat0805 (2019).
3. Villar, E. A. et al. How proteins bind macrocycles. *Nat. Chem. Biol.* **10**, 723–731 (2014).
4. Segawa, Y. et al. Synthesis of a Möbius carbon nanobelt. *Nat. Synth.* **1**, 535–541 (2022).
5. Martí-Centelles, V., Pandey, M. D., Burguete, M. I. & Luis, S. V. Macrocyclization reactions: the importance of conformational, configurational, and template-induced preorganization. *Chem. Rev.* **115**, 8736–8834 (2015).
6. Girvin, Z. C., Andrews, M. K., Liu, X. & Gellman, S. H. Foldamer-templated catalysis of macrocycle formation. *Science* **366**, 1528–1531 (2019).
7. Sytniczuk, A. et al. At long last: olefin metathesis macrocyclization at high concentration. *J. Am. Chem. Soc.* **140**, 8895–8901 (2018).
8. O'Sullivan, M. C. et al. Vernier templating and synthesis of a 12-porphyrin nano-ring. *Nature* **469**, 72–75 (2011).
9. Zheng, K. & Hong, R. Stereoconfining macrocyclizations in the total synthesis of natural products. *Nat. Prod. Rep.* **36**, 1546–1575 (2019).
10. Gagnon, C. et al. Biocatalytic synthesis of planar chiral macrocycles. *Science* **367**, 917–921 (2020).
11. Mori, K., Ohmori, K. & Suzuki, K. Hydrogen-bond control in axially chiral styrenes: selective synthesis of enantiomerically pure C_2 -symmetric paracyclophanes. *Angew. Chem. Int. Ed. Engl.* **48**, 5638–5641 (2009).
12. Wang, J. & Feringa, B. L. Dynamic control of chiral space in a catalytic asymmetric reaction using a molecular motor. *Science* **331**, 1429–1432 (2011).
13. Romanazzi, G., Degennaro, L., Mastroilli, P. & Luisi, R. Chiral switchable catalysts for dynamic control of enantioselectivity. *ACS Catal.* **7**, 4100–4114 (2017).
14. Ojima, I. *Catalytic Asymmetric Synthesis* (John Wiley & Sons, 2010).
15. Bierschenk, S. M. et al. Impact of host flexibility on selectivity in a supramolecular host-catalyzed enantioselective aza-Darzens reaction. *J. Am. Chem. Soc.* **144**, 11425–11433 (2022).
16. Nishioka, Y., Yamaguchi, T., Kawano, M. & Fujita, M. Asymmetric [2 + 2] olefin cross photoaddition in a self-assembled host with remote chiral auxiliaries. *J. Am. Chem. Soc.* **130**, 8160–8161 (2008).
17. Yu, Y., Yang, J. M. & Rebek, J. Molecules in confined spaces: reactivities and possibilities in cavitands. *Chem* **6**, 1265–1274 (2020).
18. Brown, C. J., Bergman, R. G. & Raymond, K. N. Enantioselective catalysis of the aza-cope rearrangement by a chiral supramolecular assembly. *J. Am. Chem. Soc.* **131**, 17530–17531 (2009).
19. Sun, B. et al. Asymmetric transformation driven by confinement and self-release in single-layered porous nanosheets. *Angew. Chem. Int. Ed. Engl.* **59**, 22690–22696 (2020).
20. Wang, K., Jordan, J. H., Hu, X. & Wang, L. Supramolecular strategies for controlling reactivity within confined nanospaces. *Angew. Chem. Int. Ed. Engl.* **59**, 13712–13721 (2020).
21. Lu, Z. et al. Enantioselective fullerene functionalization through stereochemical information transfer from a self-assembled cage. *Nat. Chem.* **15**, 405–412 (2023).
22. Korevaar, P. A. et al. Pathway complexity in supramolecular polymerization. *Nature* **481**, 492–496 (2012).
23. Matern, J., Dorca, Y., Sánchez, L. & Fernández, G. Revising complex supramolecular polymerization under kinetic and thermodynamic control. *Angew. Chem. Int. Ed. Engl.* **58**, 16730–16740 (2019).
24. Wehner, M. et al. Supramolecular polymorphism in one-dimensional self-assembly by kinetic pathway control. *J. Am. Chem. Soc.* **141**, 6092–6107 (2019).
25. Kim, Y. J. et al. Collective helicity switching of a DNA-coat assembly. *Nat. Nanotechnol.* **12**, 551–556 (2017).
26. Zhao, H. et al. Reversible trapping and reaction acceleration within dynamically self-assembling nanoflasks. *Nat. Nanotechnol.* **11**, 82–88 (2016).
27. Fanlo-Virgos, H., Alba, A. R., Hamieh, S., Colomb-Delsuc, M. & Otto, S. Transient substrate-induced catalyst formation in a dynamic molecular network. *Angew. Chem. Int. Ed. Engl.* **53**, 11346–11350 (2014).
28. Wang, H., Wang, Y., Shen, B., Liu, X. & Lee, M. Substrate-driven transient self-assembly and spontaneous disassembly directed by chemical reaction with product release. *J. Am. Chem. Soc.* **141**, 4182–4185 (2019).
29. Gulder, T. & Baran, P. S. Strained cyclophane natural products: macrocyclization at its limits. *Nat. Prod. Rep.* **29**, 899–934 (2012).
30. Sun, B. et al. Homochiral porous nanosheets for enantiomer sieving. *Nat. Mater.* **17**, 599–604 (2018).
31. Legrand, Y., Van der Lee, A. & Barboiu, M. Single-crystal X-ray structure of 1,3-dimethylcyclobutadiene by confinement in a crystalline matrix. *Science* **329**, 299–302 (2010).
32. Zigon, N., Duplan, V., Wada, N. & Fujita, M. Crystalline sponge method: X-ray structure analysis of small molecules by post-orientation within porous crystals—principle and proof-of-concept studies. *Angew. Chem. Int. Ed. Engl.* **60**, 25204–25222 (2021).

Acknowledgements

This work was supported by National Natural Science Foundation of China (grant nos. 21971084, 92156023 and 22150710515, to M.L., and 22171052, to M.S.), Science and Technology Commission of Shanghai Municipality (22520712300 and 23WZ2501000, to M.S.) and Fudan University Fund (to M.L. and M.S.). We thank Y. Kim for helpful discussion on simulations.

Author contributions

L.T., H.W. and J.W. synthesized molecules and performed spectroscopic measurements and TEM experiments. L.T. and M.S. performed HPLC experiments for chiral macrocyclizations to quantify conversion and enantioselectivity. M.S. performed CD experiments, AFM measurements and dynamics simulation. J.K. performed X-ray experiments. M.L. developed the concept, supervised the research and wrote the manuscript with input from all authors.

Competing interests

The authors declare no competing interests.

Additional information

Supplementary information The online version contains supplementary material available at <https://doi.org/10.1038/s44160-023-00360-0>.

Correspondence and requests for materials should be addressed to Mo Sun or Myongsoo Lee.

Peer review information *Nature Synthesis* thanks Niveen Khashab and the other, anonymous, reviewer(s) for their contribution to the peer review of this work. Primary Handling Editor: Alison Stoddart, in collaboration with the *Nature Synthesis* team.

Reprints and permissions information is available at www.nature.com/reprints.

Publisher's note Springer Nature remains neutral with regard to jurisdictional claims in published maps and institutional affiliations.

Springer Nature or its licensor (e.g. a society or other partner) holds exclusive rights to this article under a publishing agreement with the author(s) or other rightsholder(s); author self-archiving of the accepted manuscript version of this article is solely governed by the terms of such publishing agreement and applicable law.

© The Author(s), under exclusive licence to Springer Nature Limited 2023